How Cells Tiptoe on Adhesive Surfaces before Sticking

Anne Pierres,*†‡§ Anne-Marie Benoliel,*†‡§ Dominique Touchard,*†‡§ and Pierre Bongrand*†‡§

*INSERM UMR600, †CNRS UMR6212, ‡Université de la Mediterranée, and §APHM, Laboratoire "Adhésion et Inflammation",
Campus de Luminy, Case 937, 13288 Marseille cedex 09, France

ABSTRACT   Cell membranes are studded with protrusions that were thoroughly analyzed with electron microscopy. However, the nanometer-scale three-dimensional motions generated by cell membranes to fit the topography of foreign surfaces and initiate adhesion remain poorly understood. Here, we describe the dynamics of surface deformations displayed by monocytic cells bumping against fibronectin-coated surfaces. We observed membrane undulations with typically 5 nm amplitude and 5–10 s lifetime. Cell membranes behaved as independent units of micrometer size. Cells detected the presence of foreign surfaces at 50 nm separation, resulting in time-dependent amplification of membrane undulations. Molecular contact then ensued with apparent cell-membrane separation of 30–40 nm, and this distance steadily decreased during the following tens of seconds. Contact maturation was associated with in-plane egress of bulky molecules and robust membrane fluctuations. Thus, membrane undulations may be the major determinant of cell sensitivity to substrate topography, outcome of interaction, and initial kinetics of contact extension.

INTRODUCTION

The contact between a cell and a foreign surface often triggers a variety of events such as cell attachment, spreading on the surface, and alteration of behavioral patterns relative to survival, differentiation, migration, or release of bioactive factors (1). During the last years, the biologically relevant phenomena occurring after the first minutes after cell-to-surface encounter were subjected to considerable scrutiny. Also, much effort was done to apply biophysical approaches to the analysis of the binding events occurring during the first seconds after contact (2–4). However, fewer studies were specifically focused on the first minutes after cell-to-surface contact and preceding biologically relevant responses such as spreading, lamellipodium formation, and migration or activation of different functions. Interestingly, recent experiments performed with atomic force microscopy at the single-cell level (5) suggest that cell adhesion to a surface may sequentially involve passive formation of a few receptor-ligand bonds followed a few minutes later by active cooperative events resulting in more than a 10-fold increase of adhesive strength. Thus, it is warranted to investigate the minute-scale period linking cell-substrate encounter to generation of an active response guided by specific recognition events involving cell membrane receptors and substrate molecular structures.

Numerous electron microscopical studies clearly demonstrated that cell membranes are studded with different membrane folds or protrusions such as microvilli, lamellipodia, or filopodia (6–8). Cell adhesion is essentially mediated by membrane receptors of typically several tens of nanometer length (9); this is significantly shorter than the smallest protrusions covering the cell membrane, because microvilli are several tenths of a micrometer long (8). Thus, formation of a substantial contact area on the order of several squared micrometers (10) requires nanometer-scale fitting of the cell topography to opposing surfaces. Indeed, although contact formation between a rough cell membrane and a smooth surface obviously requires a minimal smoothing of the cell surface, (11), intercellular adhesion also requires membrane adaptation (12).

Whereas aforementioned requirements were fully illustrated with electron microscopy, little information is currently available on the dynamics of cell membrane at the nanometer scale. It has long been shown that the surface of erythrocytes (13) or deflated lipid vesicles display thermally driven oscillations, and much theoretical work was devoted to account for this phenomenon (14,15). However, little information is available on the dynamics of nucleated cell membranes at the submicrometer level. Transverse oscillations of up to 20–30 nm amplitude were found on many nucleated cells such as fibroblasts, lymphocytes, or monocytes (16–18). Other studies (8) revealed that leukocyte surface microvilli could withstand a pulling force of ~45 nN before forming a thin membrane tether. However, more work is needed to understand the relationship between membrane undulations and the early steps of contact formation and extension between a cell and an adhesive surface.

The purpose of this work was to provide a real-time description of three-dimensional membrane deformations occurring during the first tens of seconds required to secure cell attachment to adhesive surfaces. We used interference reflection microscopy/reflection interference contrast microscopy (IRM/RICM) (18–22) to image the initial interaction between human monocytic THP-1 cells and planar fibronectin-coated surfaces. Cell membranes displayed continuous transverse undulations of nanometer amplitude with a lateral correlation

on the order of a micrometer. Cells seemed to detect the presence of the surface at ~50 nm separation as revealed by the behavior of membrane fluctuations. Adhesion was not an immediate phenomenon; instead, the cell-to-surface gap decreased by several tens of nanometers during the first few minutes after initial contact. This contact maturation occurred concomitantly with an egress of bulky components of the cell glycocalyx. Observation of cytoskeletal elements suggested that actin acted at least partly as a stabilizing structure, and myosin was not detectable in contact areas.

MATERIALS AND METHODS

Cells and transfection

We used the monocytic THP-1 line (23) maintained as previously described (24) in Roswell Park Memorial Institute-1640 medium (Invitrogen) supplemented with 20 mM HEPES buffer, 10% fetal calf serum (Invitrogen, Cergy Pontoise, France), 2 mM L-glutamine, 50 U/ml penicillin, and 50 μg/ml streptomycin. As previously checked with flow cytometry, these cells expressed typical mononuclear phagocyte markers including CD11b, CD18, CD29, CD32, CD43, CD45, CD64, and class I major histocompatibility complex molecules. They also were shown to bind fibronectin-coated surfaces with CD49dCD29 (VLA-4) and CD49eCD29 (VLA-5) integrins (24).

THP-1 cells were transfected with pEGFP-actin (Clontech, BD Biosciences, Mountain View, CA) using an Amaxa (Kolin, Germany) electroporator, Amaxa solution V, and protocol V-01. EGFP-positive cells were selected with G418 selection and limiting dilution plating to isolate clones that were stably expressing EGFP-actin. For transfected cells, 1mg/ml G-418 sulfate (GIBCO, Invitrogen) was added in culture medium.

Fluorescent labeling and metabolic inhibitors

Cell overall shape was studied by monitoring cells suspended in culture medium containing 10 μg/ml fluorescein isothiocyanate with confocal microscopy.

In other experiments, cells were labeled with anti-CD43 monoclonal and processed for zenon labeling per process manufacturer (Molecular Probes, Eugene, OR) procedure. Mouse anti-CD29 (K20) and anti-CD45 were purchased from Beckman Coulter (Miami, FL). Cytochalasin D (an inhibitor of microfilament assembly) and butanedione monoxime (a myosin inhibitor) were obtained from Sigma (St. Louis, MO). Intracellular calcium visualization was achieved after labeling cells with Fluo-3-AM (Molecular Probes), as previously described (25).

Chambers

Custom-made flow chambers (Satim, Evenos, France) were plexiglas blocks drilled with a rectangular cavity of $17 \times 6 \times 1$ mm^3 and cylindrical ducts for liquid entry and exit. The chamber floor was made of a glass coverslip maintained against the cavity with a steel plate.

Coverslips were cleaned by treatment with 98% sulfuric acid for 4 h, washed overnight with running tap water, then distilled water, and dried at 60°C for 30 min. They were then treated with 10 μg/ml fibronectin (Sigma) for 2 h and rinsed in phosphate-buffered saline.

Chambers were set on the stage of an Axiovert 135 inverted microscope (Zeiss, Oberkochen, Germany) bearing a heating stage (TRZ 3700) set at 37°C. IRM was performed with an antiflex objective (63× magnification, 1.25 numerical aperture). Illumination was performed with a 50 watt mercury lamp using a H546 band-pass filter. Images were obtained with an Hamamatsu (Massy, France) C4742-95-10 CCD camera yielding 10-bit accuracy. Pixel size was 125×125 nm^2.

Spreading assays were initiated by injecting 10 μl of a concentrated cell suspension (2×10^6 cells/ml) into the bottom of treated chambers containing normal culture medium. In a typical experiment, 300 sequential images were recorded with ~1 Hz frequency.

Image processing

Image processing was performed with a custom-made C++ Window compatible software written in the laboratory. This allowed us to perform the following key steps as an improvement of a previously described and validated procedure (22):

The first step consisted of performing a first order linear correction of brightness with respect to coordinates to minimize the illumination differences between the four corners of a 25×25 μm^2 area surrounding the cell. The same correction parameters were used throughout each series of 300 images, because they were essentially dependent on the cell position with respect to the microscope field.

Second, the local intensity at each pixel was replaced with the average of intensities measured on the neighboring 5×5 pixels. This was chosen to reduce the image noise sufficiently to decrease the height measurement error below ~1 nm, which was found necessary to process cell images. Note that the loss of lateral resolution did not result in dramatic loss of information compared with the maximum resolution yielded with IRM/RICM.

The last step consisted of deriving a relative membrane to substrate distance z from the brightness I in the equation

$$z = (\lambda/4\pi) \, \text{Arccosine} \left[(2I - I_{\mathrm{m}} - I_{\mathrm{M}})/(I_{\mathrm{m}} - I_{\mathrm{M}}) \right], \quad (1)$$

where λ is the light wavelength, and I_{m} and I_{M} are the minimum and maximum brightness, respectively, corresponding to contact and $(\lambda/4)$ separation. The importance of this formula is that estimates may be considered as fairly robust even if underlying assumptions are not fully warranted (22). Note also that the ambiguity linked to the arccosine transform is not a problem when we consider only a region close to the contact where the membrane-to-surface distance is expected to remain lower than ~100 nm. This assumption is supported by the absence of concentric fringes usually observed on the rim of molecular contact zones (21,22,26).

Parameters I_{m} and I_{M} were determined after examining a set of 300 images on the same microscope field. Corrected values were used for each image to account for the fluctuations of illumination intensity of a fixed empty area (the coefficient of variation was close to 1%).

Note that this procedure was not expected to yield absolute distances. However, it must be recognized that there is a necessary arbitrariness in defining a nanometer-scale distance between surfaces coated with macromolecules of various shapes.

The results presented in this article were obtained after examining ~5000 microscope fields of ~125×125 μm^2 each.

RESULTS

Cells adhere to adhesive surfaces and form growing contacts within <1 min

Monocytic THP-1 cells were deposited on fibronectin-coated surfaces in a chamber set on a microscope stage. Although these cells were fairly spherical in suspension, they displayed marked flattening at the micrometer scale within seconds after contact (Fig. 1 A). Interference reflection microscopy/reflection interference contrast microscopy (IRM) was used to image the details of the cell surface in front of the
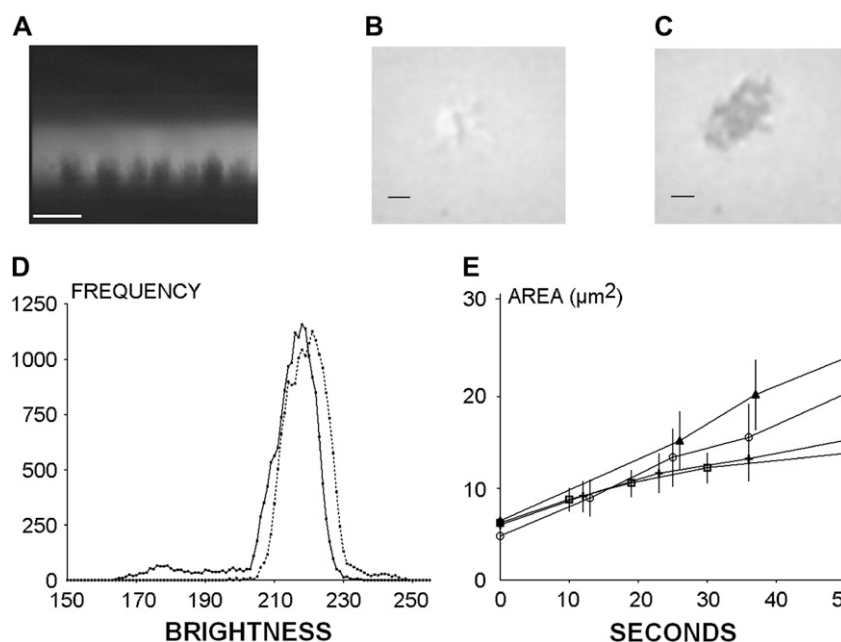
FIGURE 1 Imaging contact formation between a cell and an adhesive surface. (*A*) A spherical THP-1 cell deposited on a surface flattens within seconds as revealed with confocal microscopy in fluorescent medium. White bar length, 25 μm. (*B*) The cell surface first appears fairly bright with interference reflection contrast microscopy. Bar length, 2 μm. (*C*) A total of 71 s later, an extensive contact zone is visible as a dark area with IRM/RICM. Bar length, 2 μm. (*D*) Comparing the brightness histograms of the images in *B* (*dashed line*) and *C* (*solid line*) allows objective definition of contact zone with a cutoff intensity value ($\downarrow$). (*E*) THP-1 cells were deposited on adhesive surfaces treated with different concentrations of fibronectin, and the rate of contact growth was determined. Surfaces were derivatized with fibronectin solutions at 0.1 μg/ml ($\square$), 1 μg/ml (+), 10 μg/ml ($\blacktriangle$), and 100 μg/ml ($\bullet$). Error bars represent mean $\pm$ SE of 15 to 25 separate cells.

substratum with nanometer vertical resolution. As shown on Fig. 1, *B* and *C*, within a few tens of second after contact, a dark area appeared on the IRM image of the cell surface, revealing the formation of a contact zone with surface separation less than several tens of nanometers. This was previously shown to reflect bona fide adhesion (22). Comparing the histograms of images obtained before and after adhesion (Fig. 1 *D*) allowed us to define a threshold intensity (Fig. 1 *D*, *arrow*) to define contact zones and measure adhesive areas. as was done in previous reports (10,21,27). The corresponding separation value obtained with Eq.1 was 34 nm. The kinetics of contact extension was then studied. As shown on Fig. 1 *E*, contact area first increased linearly with respect to time, and the growth rate was weakly dependent on surface concentration of adhesion molecules. This finding is consistent with the concept that contact extension should be essentially driven by cell movements, without any requirement for cooperative interactions between membrane receptors (5,28).

As exemplified in Fig. 2, *A–I*, growing contact zones exhibited two important features: 1), the contact patches appeared fairly irregular, and 2), some isolated patches sometimes appeared and disappeared, demonstrating the need to consider three-dimensional membrane topography to account for two-dimensional contact growth.

Cell-substrate contact formation is associated with transverse membrane deformation and fluctuations of contact area superimposed on a continuous decrease of membrane-to-substrate distance

IRM images were processed to estimate cell-to-substrate distance within the 100 nm range. Images of cells falling on planar fibronectin-coated surfaces were recorded for periods

of 5 min with 1 Hz frequency. Three sequential, color-coded, maps of cell-surface distance are displayed in Fig. 3, *A–C*, corresponding to the two-dimensional representations displayed in Fig. 2, *A–C*: clearly, contact formation was preceded with important cell surface deformations. These deformations were also displayed on Fig. 4 with a more intuitive three-dimensional representation. Thus, contact initiation and extension were correlated with continuous membrane fluctuations. As shown in Fig. 5, these membrane undulations appeared concomitantly with two phenomena: 1), contact area displayed marked fluctuations with ~0.1 Hz frequency, which were superimposed on average growth (Fig. 5 *A*), and 2), during several tens of seconds after cell-to-surface contact, the relative molecular distance between interacting surfaces within previously defined contact zones steadily decreased by at least 30 nm (Fig. 5 *B*). Thus membrane adhesion in a given point is not an all-or-none instantaneous process, but this process involves progressive narrowing of the cell-surface gap.

Transverse membrane fluctuations may be described as a vertical motion of blocks of 0.6 μm width and an effective diffusion coefficient of 1–3 nm^2/s

A conventional display of contact fluctuations is shown in Fig. 6 *A*, emphasizing the concomitant expansion and retraction of contact in different zones. This two-dimensional view is a consequence of three-dimensional deformations of the cell membranes (Fig. 6 *B*): different regions of the cell membrane facing the substratum displayed upward or downward displacements of 5–10 nm amplitude in different regions of the cell membrane during a 6 s period of time. These overall displacements were associated with membrane fluctuations
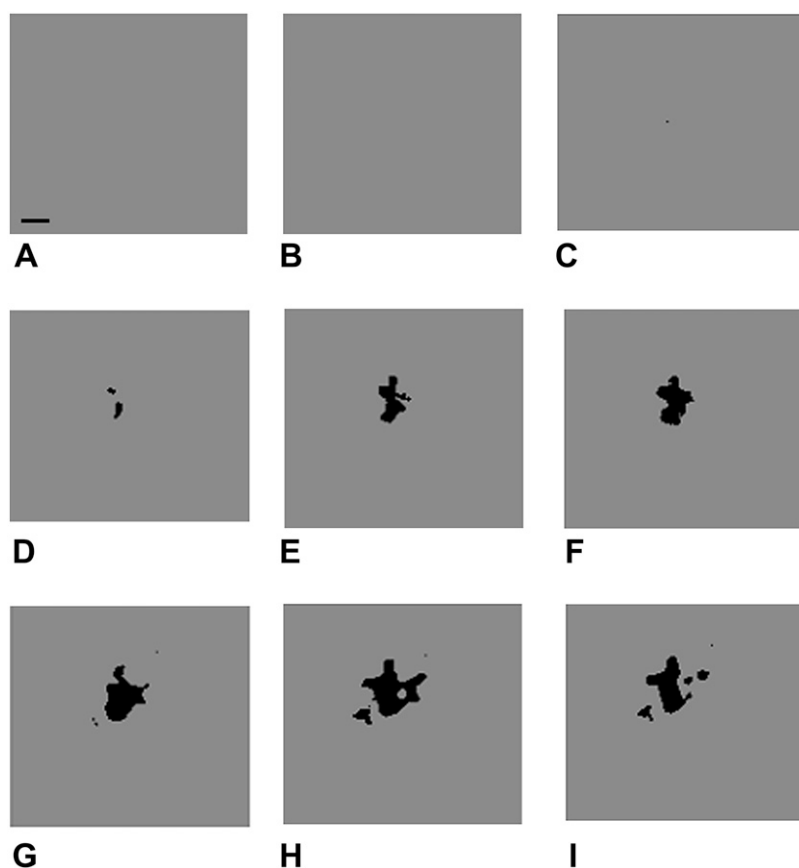
FIGURE 2 Typical pattern of growing contact area. (*A–I*) Monocytic THP-1 cells were deposited on a surface treated with 10 μg/ml fibronectin. A microscope field was selected before the onset of the experiment, and the cell-surface contact regions (corresponding to <34 nm apparent separation between surfaces) were determined at regular intervals of 9 s, which are shown as black areas. Bar length is 2 μm.

that were revealed by imaging the standard deviation of the *z* coordinate on each pixel during the same period of time and using higher frequency image acquisition (Fig. 6 *C*). Then, to understand the rationale of cell shape control, the following analysis was performed:

1). We examined the randomness of membrane deformations by studying the time dependence of the squared displacements of individual surface pixels. Indeed, random walks result in a linear dependence of squared displacement on time, whereas a uniform motion would lead to a linear relationship between displacement and time. As exemplified in Fig. 7 *A*, when the mean membrane approach to the surface was subtracted from individual pixel displacement, the relationship between squared displacement and time was

strikingly linear. This finding was obtained on nine separate cells and time intervals ranging between 6 and 80 s, immediately after contact, yielding an effective diffusion coefficient equal to half the slope of the curves (because the squared displacement during time *t* is expected to be equal to $2\,Dt$). This ranged between ~1–3 nm^2 per second. Thus, membrane fluctuations separated by a 1 s period of time were not correlated. Further information was obtained by studying the temporal autocorrelation of membrane shape and fluctuation maps. As exemplified in Fig. 7 *B*, the characteristic time for 50% decrease of correlation was ~5 s during contact initiation. However, the onset of adhesion resulted in progressive increase of correlation as a consequence of the formation of fixed adhesive zones
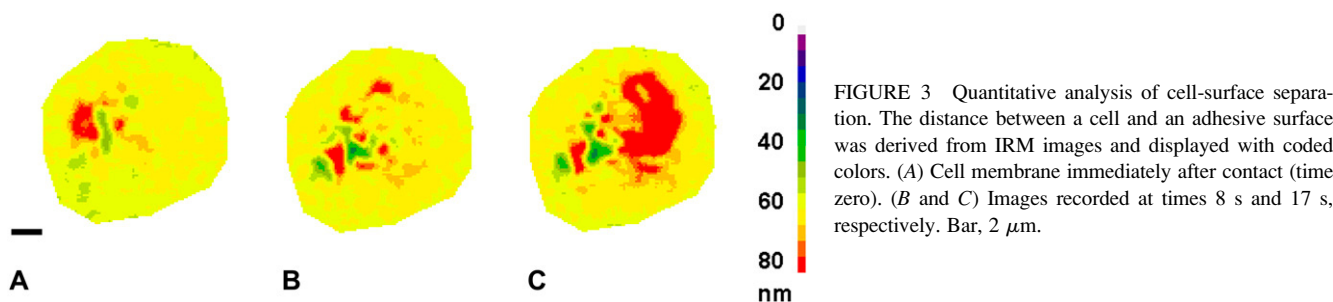

FIGURE 3 Quantitative analysis of cell-surface separation. The distance between a cell and an adhesive surface was derived from IRM images and displayed with coded colors. (*A*) Cell membrane immediately after contact (time zero). (*B* and *C*) Images recorded at times 8 s and 17 s, respectively. Bar, 2 μm.
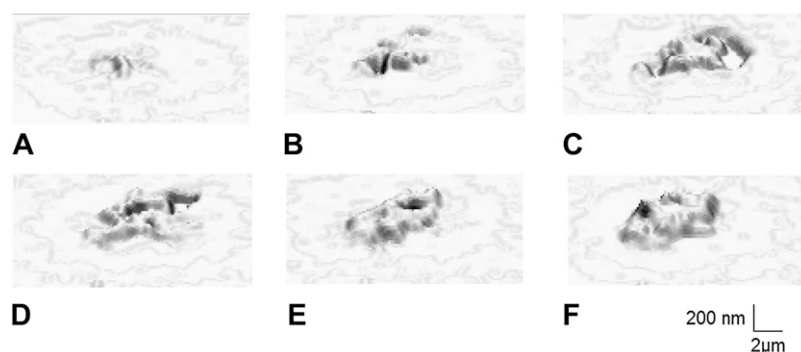
FIGURE 4 Three-dimensional image of the topography of the membrane zone facing an adhesive surface. The shape of the cell described in Fig. 3 is shown at times 0, 8, 17, 26, 35, and 64 s, respectively, in *A–F*.

(not shown). We also studied the time correlation of displacements (i.e., of the time derivative of membrane maps). No correlation could be found between sequential displacements (Fig. 7 *B*). Together with Fig. 6 *A*, this is consistent with the view that the characteristic duration of membrane fluctuations was significantly <1 s, but a longer correlation was generated by the formation of adhesive patches.

2). Then we examined the dependence of the amplitude of membrane fluctuations on the z coordinate (i.e., distance to the adhesive substrate). Indeed, passive surface undulations of soft vesicles have long been studied (14,15), and the squared amplitude of undulations should be decreased by a neighboring surface in proportion to the squared distance (29). The mean correlation coefficient between distance to the fibronectin-coated surface and undulation amplitude calculated on a series of 16 different images was 0.101 ($\pm$0.358 SD). The significance of this unexpectedly low correlation was explained by plotting fluctuations (expressed as a standard deviation) versus distance. As exemplified in Fig. 7 *C*, a nonmonotonous relationship between the local z coordinate and fluctuation amplitude was found. Two domains were apparent:

For higher distances ($z > 70$ nm), the fluctuation strongly increased as a function of distance, in accordance with predictions from the theory of statistical surfaces.

When z became $< \sim 50$ nm, fluctuations no longer decreased concomitantly. Interestingly, during the first tens of seconds after contact, low-distance fluctuations increased, supporting the biological relevance of this finding.

3). Examining deformation and fluctuation maps such as Fig. 6, *B–C*, clearly revealed the heterogeneity of surface movement distribution, with a coexistence of more active and quieter membrane regions. The characteristic size of these areas was determined by studying spatial autocorrelation. A typical plot is displayed in Fig. 7 *D*. The mean length for 50% correlation decay determined on 16 separate cell images was 0.60 μm (0.45 μm SD). Accordingly, a comparable correlation length was found on the maps of individual pixel displacements during a fixed period of 2 s, suggesting that cell membranes might deform as independent units of nearly micrometer size.

Contact extension is correlated to important changes of cytoplasmic and surface molecules

To obtain more information on the structural basis of observed phenomena, fluorescence microscopy was associated
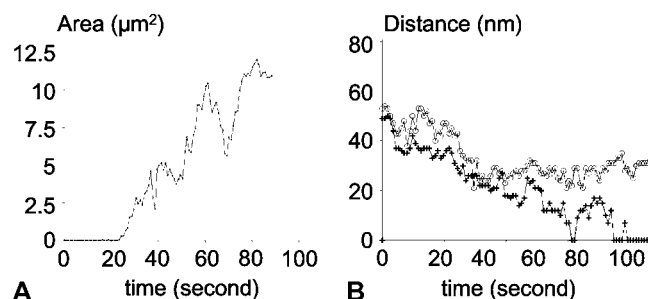

FIGURE 5 Quantitative parameters of contact extension and tightening. (*A*) The contact area determined on a single cell is shown, disclosing fluctuations that were not visible on mean curves displayed in Fig. 1 *E*. (*B*) The distance between a fixed point of the cell membrane ($\bigcirc$) and the minimum distance between the cell surface and the adhesive plane (*crosses*), revealing progressive decrease of the distance between surfaces. This representative pattern was found with a similar timescale on 12 different cells.
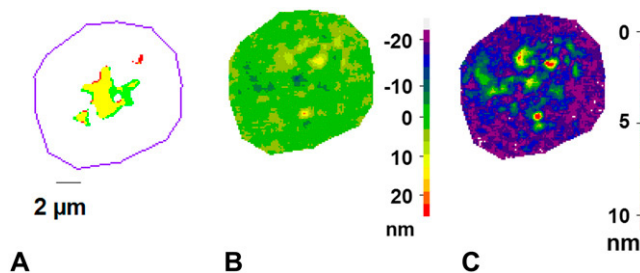

FIGURE 6 Imaging cell membrane undulations. (*A*) The contact evolution during a 5.6 s period of time is shown on a representative cell. Whereas the region of stable contact is displayed in yellow, gain and loss of adhesive zone are displayed in red and green. (*B*) The overall vertical membrane displacement is displayed with coded colors. (*C*) The amplitude of vertical membrane undulations is displayed as the standard deviation of eight sequential values of the z coordinate, revealing the random part of the deformation.
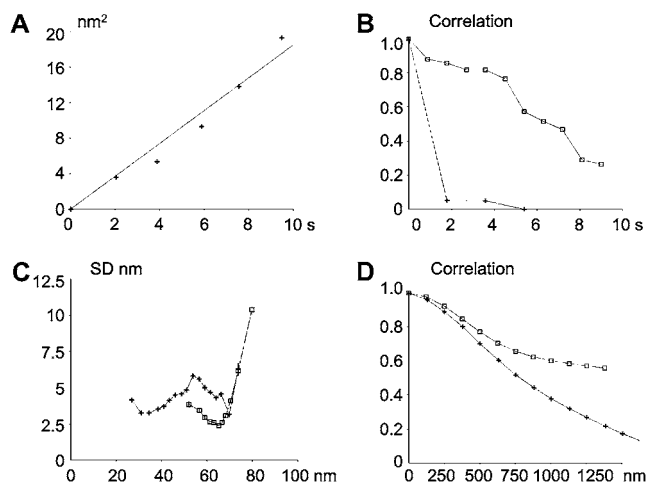
FIGURE 7 Quantitative description of cell membrane transverse fluctuations during contact extension. (*A*) A representative cell imaged with ~1 Hz frequency during contact formation. The squared displacement per pixel was plotted versus time after subtracting the overall displacement (corresponding to decrease of average cell-to-surface distance). The plot is fairly linear. Correlation coefficient is 0.991. (*B*) Lifetime of membrane undulations: the time dependence of correlation between two sequential membrane maps (□) on a typical cell reveals 50% decrease of correlation during ~8 s. Crosses represent displacements of a given membrane point reveal no detectable temporal correlation, suggesting that membrane deformations are driven by random movements with higher that 1 Hz frequency (in line with Fig. 3 *B*). (*C*) Dependence of the amplitude of vertical membrane displacements (as imaged in Fig. 6 *C*) on distance to the adhesive surface. Squares represent onset of contact. Crosses represent 130 s after contact initiation. *D* shows correlation length of cell contour. Both membrane images (□) and local displacements during a 2.7 s interval (*crosses*) display marked spatial correlation with a 50% decrease at 1 μm separation.

with IRM to study the short-term cell structural changes after formation:

First, fluorescent antibodies were made to bind beta 1 integrins, i.e., the adhesion receptors mediating THP-1 cell attachment to fibronectin (24). High fluorescence levels were observed in cell-surface contact areas (not shown), but more extensive investigations are required to determine whether the surface density of integrins increased during contact maturation.

Second, we labeled CD43, which is a bulky membrane molecule that is highly abundant on leukocyte membranes and that is supposed to impair adhesive interactions (30,31). Interestingly, as exemplified in Fig. 8, decrease of cell-to-substrate distance was associated with a concomitant egress of CD43 molecules.

Third, THP-1 cells were transfected with fluorescent actin and deposited on fibronectin-coated surfaces. Contact formation was very similar to processes described above, suggesting that transfection did not markedly alter THP-1 cell properties. The fluorescence distribution was then monitored together with IRM contacts. As exemplified in Fig. 9, in addition to bulk fluorescence,
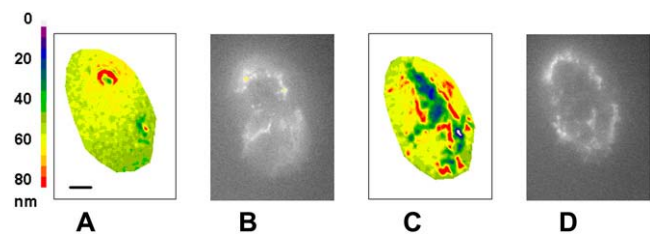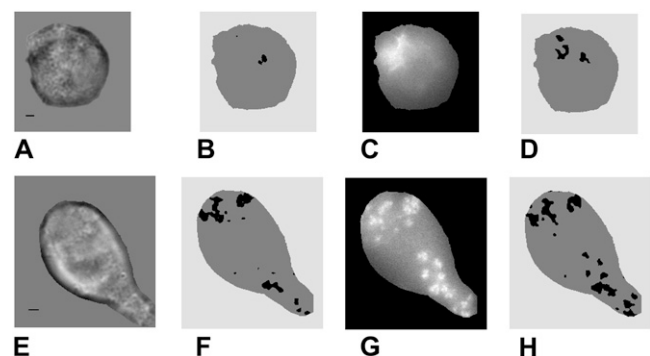

FIGURE 8 Leukosialin redistribution during contact formation. Monocytic THP-1 cells were labeled with fluorescent anti-CD43/leukosialin before deposition on fibronectin-coated surfaces. Fluorescence and IRM images were then recorded at regular intervals. During the first minute, the separation between the cell membrane and the adhesive surface is nearly always >35 nm (*A*), and CD43 is clearly visible on the whole surface, with local concentration (*B*, ↑). A total of 60 s later, cell-surface distance decreased by at least 20 nm (*C*, ↑) and CD43 depletion is clearly visible in the whole cell surface and, particularly, in the new contact zone (*D*).

cells displayed localized fluorescence patches that seemed to appear a few tens of seconds before the formation or extension of contact zones.

Metabolic inhibitors influence contact extension

Whereas it is well known that soft vesicles can display thermally driven surface fluctuations and the formation of extensive contacts with adhesive surfaces, it was important to determine the extent to which cell behavior was influenced by active processes dependent on biochemical events. This question was addressed as follows:

i). Stiffening cell surface with paraformaldehyde abolished contact formation and adhesion.

FIGURE 9 Actin redistribution during contact formation. Monocytic THP-1 cells were transfected with GFP before being deposited on fibronectin-coated surfaces, and contact regions were analyzed with IRM and fluorescence. Two representative sets of images (*A–D* and *E–H*) are shown. (*A*) Visible light image of a standard cell (with usual roundish appearance preceding spreading). *B* and *D* display contact growth during a 90 s period of time. On the fluorescence image (*C*), actin appears distributed throughout the whole cell, with local bright patches (↑) that were associated with, and seemed to precede, contact. (*E–H*) A similar behavior was observed several minutes after initial contact, on a markedly polarized cell.

ii). Interestingly, treating cells with moderate concentrations of cytochalasin D (10 μg/ml) resulted in significant decrease of the rate of contact extension; smoothening of the two-dimensional contours of contact surfaces, which make them more alike contact zones formed with artificial vesicles (11,24); and increase of membrane undulations in membrane zones close to the adhesive surface (Fig. 10).

iii). Treating cells with a myosin inhibitor (butanedionemonoxime) to decrease cell motility abolished adhesion and contact formation.

iv). Because previous reports clearly demonstrated a role of intracellular calcium changes in cell spreading (32,33), we investigated whether intracellular calcium level influenced THP-1 cell fitting to adhesive surfaces. In preliminary experiments, cells were labeled with fluo-3, a fluorescent calcium probe, before deposition on fibronectin-coated surfaces and monitoring with IRM. Whereas many cells displayed elevated calcium, no clear relationship was found between intracellular calcium and rate of contact growth (not shown).

The requirement for fluid drainage from the cell-surface gap does not seem to be a limiting parameter for contact extension

In several situations of physical interest (e.g., aquaplaning) adhesion between surfaces may be hampered by intervening liquid film. The possibility that this might influence contact extension was investigated by monitoring contact extension in highly viscous Ficoll solution. However, no significant decrease of contact extension was found when the medium viscosity was increased threefold (not shown).
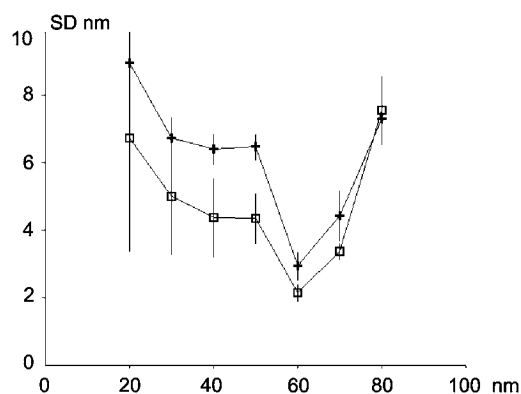

FIGURE 10 Effect of cytochalasin D on membrane fluctuations near a surface. Seven control cells ($\square$) and eight cytochalasin D-treated cells ($+$) were monitored for determination of membrane topographical and fluctuation maps. The standard deviation of membrane height, representing a fluctuation amplitude, was determined on separate groups of point with common distance to the surface. Cytochalasin treatment did not substantially influence fluctuations at 60–80 nm separation, but this seemed to increase fluctuations for smaller distances (the difference was significant for 50 nm separation with Student's t-test).

DISCUSSION

Although cell attachment to adhesive surfaces and subsequent deformation and spreading were subjected to considerable scrutiny, little information is available on the mechanisms allowing transverse nanometer-scale adaptation of interacting surfaces. However, in view of the known roughness of cell membranes and the length of adhesion molecules, this fitting process seems an obvious requirement for the formation of more than a few adhesive bonds. This point is important, because previous studies performed on the strength of cell adhesion suggested that the minimal number of bonds required to account for experimental properties of cell adhesion was on the order of about at least 1000 (34,35).

IRM/RICM was demonstrated to be a method of choice to image the fitting of cell membranes to planar surfaces with sufficient vertical resolution (18,19,22,26). A major advantage of this technique is that it does not require any potential artifactual treatment. It has been well recognized that the quantitative derivation of membrane-surface distance from intensity measurements relies on several assumptions that are difficult to prove (36), and the membrane-surface separation values we obtained may not be considered as absolute values of the distance between lipid bilayers and glass surfaces. However, it must be emphasized that the simple procedure we used to derive these distances is fairly robust and should provide reliable relative values, as acknowledged in previous studies (18,20,22). Indeed, cytoplasmic structures such as the actin cortex might influence image brightness. Although our observations of the kinetics of actin and distance map changes suggest that actin movements were much slower than the membrane fluctuations we described, a reliable proof of the validity of distance determination with IRM/RICM could only be obtained by comparing images obtained with different techniques. We are currently combining total internal reflection fluorescence microscopy and fluorescence labeling to achieve this goal.

Several important conclusions may be drawn from our experiments. First, in addition to the mere confirmation of previous reports demonstrating the occurrence of transverse fluctuations of nucleated cell membranes (16–18), our results provide some new information on these fluctuations. The tentative view of these fluctuations as transverse motions of micrometer-size blocks with an effective diffusion coefficient of a few nm^2/s may be useful to model these movements. Interestingly, this concept of independent motile units is consistent with previous reports on the autonomous behavior of small cytoplasmic fragments obtained from blood neutrophils (37). The patterns of cell undulations might also account for two recent findings: 1), cell spreading on surfaces bearing adhesive structures requires a minimum surface density of anchoring points (38,39); and 2), cell behavior on adhesive surfaces is markedly influenced by topography (40,41).

Second, the dependence of these fluctuations on local distance of the membrane to a surface (Fig. 7 *B*) strongly

suggests that cells perceive approaching structures at a distance of ~50 nm, resulting in an increase of oscillations in contrast with an expected behavior of passive objects (18,29,42). Thus, even the earliest period after cell encounter with a surface might involve active biological functions. Further work is needed to determine the surface molecules or the mechanisms mediating the initial interaction between cells and approaching surfaces.

Third, an important conclusion is that local membrane-to-surface adhesion is not an instantaneous process, because the separation gap progressively decreases during the first minute after attachment (Fig. 5 B). This phenomenon may be highly significant, because a recent study performed on the initial adhesion between natural killer cells and target cells suggested that the width of the intercellular gap, as estimated with electron microscopy, might influence the outcome of adhesion (i.e., killer cell activation versus inactivation) (43). Although little information is available on the dynamics of membrane tightening, it is reasonable to speculate that the egress of bulky membrane molecules such as CD43 might be a prerequisite for membrane approach. Whereas the exit of CD43 (31,44) and CD45 (45) from adhesion zones formed by immune cells is well demonstrated, the functional consequences remain incompletely understood. Indeed, these molecules may act by influencing the presence of other signaling molecules, or they may by themselves trigger important biochemical reactions (such as phosphate removal by CD45).

Fourth, there remains the need to assess the mechanisms responsible for membrane fluctuations. Although the order of magnitude of these deformations is consistent with a passive thermal mechanism (18) as analyzed by Helfrich and Servuss (14), several possible mechanisms might allow active cell processes to influence these deformations: 1), removal of bulky membrane structures and reduction of repulsive forces; 2), ensuring low enough surface tension and bending rigidity, which are recognized as key parameters of passive deformations; and 3), generation of active motion. Our findings that cytoskeletal impairment with cytochalasin D increased membrane fluctuations in regions closest to the adhesive surface and that increased contact formation was often preceded by local actin concentration would be consistent with the hypothesis that microfilament could act by stabilizing the membrane and adhesive interactions. This interpretation would be in line with a previous report (46) that detachment of surface adhesive cells might be triggered by a decrease of membrane-associated microfilaments.

In conclusion, cell membrane fitting to adhesive surfaces is an early step of cell adhesion that occurs simultaneously with transverse membrane fluctuations. Although strong evidence supports the hypothesis that these events are related by causal links, more work is required to unravel underlying molecular mechanisms.

REFERENCES

1. Pierres, A., A. M. Benoliel, and P. Bongrand. 2002. Cell fitting to adhesive surfaces: a prerequisite to firm attachment and subsequent events. *Eur. Cell. Mater.* 3:31–45.

2. Lawrence, M. B., and T. A. Springer. 1991. Leukocytes roll on a selectin at physiologic flow rates: distinction from and prerequisite for adhesion through integrins. *Cell.* 65:859–873.

3. Pierres, A., O. Tissot, B. Malissen, and P. Bongrand. 1994. Dynamic adhesion of CD8-positive cells to antibody-coated surfaces: the initial step is independent of microfilaments and intracellular domains of cell-binding molecules. *J. Cell Biol.* 125:945–953.

4. Grabovsky, V., S. Feigelson, C. Chen, D. A. Bleijs, A. Peled, G. Cinamon, F. Baleux, F. Arenzana-Seisdedos, T. Lapidot, Y. van Kooyk, R. L. Lobb, and R. Alon. 2000. Subsecond induction of alpha 4 integrin clustering by immobilized chemokines stimulates leukocyte tethering and rolling on endothelial vascular cell adhesion molecule 1 under flow conditions. *J. Exp. Med.* 192:495–505.

5. Taubenberger, A., D. A. Cisneros, J. Friedrichs, P. H. Puech, D. J. Muller, and C. M. Franz. 2007. Revealing early steps of $\alpha 2\beta 1$ integrin-mediated adhesion to collagen type I by using single-cell force spectroscopy. *Mol. Biol. Cell.* 18:1634–1644.

6. Erikson, C. A., and J. P. Trinkaus. 1976. Microvilli and blebs as sources of reserve surface membrane during cell spreading. *Exp. Cell Res.* 99:375–384.

7. Grinnell, F., M. Q. Tobleman, and I. Hackenbrock. 1976. Initial attachment of baby hamster kidney cells to an epoxy substratum. *J. Cell Biol.* 70:707–713.

8. Shao, J. Y., H. P. Ting-Beall, and R. M. Hochmuth. 1998. Static and dynamic lengths of neutrophil microvilli. *Proc. Natl. Acad. Sci. USA.* 95:6797–6802.

9. Springer, T. A. 1990. Adhesion receptors of the immune system. *Nature.* 346:425–434.

10. Cuvelier, D., M. Théry, Y.-S. Chu, S. Dufour, J. P. Thiéry, M. Bornens, P. Nassoy, and L. Mahadevan. 2007. The universal dynamics of cell spreading. *Curr. Biol.* 17:694–699.

11. Mège, J. L., C. Capo, A. M. Benoliel, and P. Bongrand. 1987. Use of cell contour analysis to evaluate the affinity between macrophages and glutaraldehyde-treated erythrocytes. *Biophys. J.* 52:177–186.

12. Foa, C., J. L. Mège, C. Capo, A. M. Benoliel, J. R. Galindo, and P. Bongrand. 1988. T-cell-mediated cytolysis: analysis of killer and target cell deformability and deformation during conjugate formation. *J. Cell Sci.* 89:561–573.

13. Brochard, F., and J. F. Lennon. 1975. Frequency spectrum of the flicker phenomenon in erythrocytes. *J. Phys.* 36:1035–1047.

14. Helfrich, W., and R. M. Servuss. 1984. Undulations, steric interaction and cohesion of fluid membranes. *Nuovo Cimento D.* 3:137–151.

15. Lipowsky, R. 1995. Generic interactions of flexible membranes. *In* Handbook of Biological Physics. R. Lipowsky and E. Sackmann, editors. Elsevier, Amsterdam. 521–602.

16. Yu, A., M. G. Krol, S. V. Levin, and A. D. Smilgavichus. 1990. Local mechanical oscillations of the cell surface within the range of 0.2–30 Hz. *Eur. Biophys. J.* 19:93–99.

17. Mittelman, L., S. Levin, and R. Korenstein. 1991. Fast cell membrane displacements in B lymphocytes. Modulation by dihydrocytochalasin B and colchicine. *FEBS Lett.* 293:207–210.

18. Zidovska, A., and E. Sackmann. 2006. Brownian motion of nucleated cell envelopes impedes adhesion. *Phys. Rev. Lett.* 96:048103.

19. Curtis, A. S. G. 1964. The mechanism of adhesion of cells to glass. *J. Cell Biol.* 20:199–215.

20. Verschueren, H. 1985. Interference reflection microscopy in cell biology: methodology and applications. *J. Cell Sci.* 75:279–301.

21. Albersdörfer, A., T. Feder, and E. Sackmann. 1997. Adhesion-induced domain formation by interplay of long-range repulsion and short-range attraction force: a model membrane study. *Biophys. J.* 73:245–257.

22. Pierres, A., P. Eymeric, E. Baloche, D. Touchard, A. M. Benoliel, and P. Bongrand. 2003. Cell membrane alignment along adhesive surfaces: active or passive mechanism? *Biophys. J.* 84:2058–2070.

23. Tsuchiya, S., M. Yamabe, Y. Yamaguchi, Y. Kobayashi, T. Konno, and K. Tada. 1980. Establishment and characterization of a human acute monocytic leukemia cell line (THP-1). *Int. J. Cancer.* 26:171–176.

24. Vitte, J., A. M. Benoliel, P. Eymeric, P. Bongrand, and A. Pierres. 2004. Beta 1 integrin-mediated adhesion may be initiated by multiple incomplete bonds, thus accounting for the functional importance of receptor clustering. *Biophys. J.* 86:4059–4074.

25. Kaplanski, G., C. Farnarier, A. M. Benoliel, C. Foa, S. Kaplanski, and P. Bongrand. 1994. A novel role for E- and P-selectins: shape control of endothelial cell monolayers. *J. Cell Sci.* 107:2449–2457.

26. Simson, R., E. Wallraff, J. Faix, J. Niewöhner, G. Gerish, and E. Sackmann. 1998. Membrane bending modulus and adhesion energy of wild-type and mutant cells of Dictyostelium lacking talin or cortex-illins. *Biophys. J.* 74:514–522.

27. Chamaraux, F., S. Fache, F. Bruckert, and B. Fourcade. 2005. Kinetics of cell spreading. *Phys. Rev. Lett.* 94:158102.

28. Garcia, A. J., and D. Boettiger. 1999. Integrin-fibronectin interactions at the cell-material interface: initial integrin binding and signaling. *Biomaterials.* 20:2427–2433.

29. Netz, R. R. 1995. Complete unbinding of fluid membranes in the presence of short-ranged forces. *Phys. Rev. E Stat. Phys. Plasmas Fluids Relat. Interdiscip. Topics.* 51:2286–2294.

30. Ardman, B., M. A. Sikorski, and D. E. Staunton. 1992. CD43 interferes with T-lymphocyte adhesion. *Proc. Natl. Acad. Sci. USA.* 89:5001–5005.

31. Soler, M., C. Merant, C. Servant, M. Fraterno, C. Allasia, J. C. Lissitzky, P. Bongrand, and C. Foa. 1997. Leukosialin (CD43) behavior during adhesion of human monocytic THP-1 cells to red blood cells. *J. Leukoc. Biol.* 61:609–618.

32. Kruskal, B. A., S. Shak, and F. R. Maxfield. 1986. Spreading of human neutrophils is immediately preceded by a large increase in cytoplasmic free calcium. *Proc. Natl. Acad. Sci. USA.* 83:2919–2923.

33. Pettit, E. J., and M. B. Hallett. 1998. Release of ''caged'' cytosolic Ca^{2+} triggers rapid spreading of human neutrophils adherent via integrin engagement. *J. Cell Sci.* 111:2209–2215.

34. Capo, C., F. Garrouste, A. M. Benoliel, P. Bongrand, A. Ryter, and G. I. Bell. 1982. Concanavalin A-mediated thymocyte agglutination: a model for a quantitative study of cell adhesion. *J. Cell Sci.* 26:21–48.

35. Bongrand, P., and G. I. Bell. 1984. Cell-cell adhesion: parameters and possible mechanisms. *In* Cell surface Dynamics: Concepts and Models.

A. S. Perelson, C. DeLisi, and F. W. Wiegel, editors. Marcel Dekker, New York. 459–493.

36. Gingell, D., and I. Todd. 1979. Interference reflection microscopy. A quantitative theory for image interpretation and its application to cell-substratum separation measurement. *Biophys. J.* 26:507–526.

37. Dyett, D. E., S. E. Malawista, P. H. Naccache, and R. I. Sha'afi. 1986. Stimulated cytokineplasts from human polymorphonuclear leukocytes mobilize calcium and polymerize actin. Cytoplasts made in cytochalasin B retain a defect in actin polymerization. *J. Clin. Invest.* 77:34–37.

38. Massia, S. P., and J. A. Hubbell. 1991. An RGD spacing of 440 nm is sufficient for integrin alpha v beta 3 -mediated fibroblast spreading and 140 nm for focal contact and stress fiber formation. *J. Cell Biol.* 114:1089–1100.

39. Calvacanti-Adam, E. A., T. Volberg, A. Micoulet, H. Kessler, B. Geiger, and J. P. Spatz. 2007. Cell spreading and focal adhesion dynamics are regulated by spacing of integrin ligands. *Biophys. J.* 92:2964–2974.

40. Dalby, M. J., S. J. Yarwood, M. O. Riehle, H. J. Johnstone, S. Affrossman, and A. S. Curtis. 2002. Increasing fibroblast response to materials using nanotopography: morphological and genetic measurements of cell response to 13-nm-high polymer demixed islands. *Exp. Cell Res.* 276:1–9.

41. Mossman, K. D., G. Campi, J. T. Groves, and M. L. Dustin. 2005. Altered TCR signaling from geometrically repatterned immunological synapses. *Science.* 310:1191–1193.

42. Marx, S., J. Schilling, E. Sackmann, and R. Bruinsma. 2002. Helfrich repulsion and dynamical phase separation of multicomponent bilayers. *Phys. Rev. Lett.* 88:138102.

43. McCann, F. E., B. Vanherberghen, K. Eleme, L. M. Carlin, R. J. Newsam, D. Goulding, and D. M. Davis. 2003. The size of the synaptic cleft and distinct distributions of filamentous actin, ezrin, CD43, and CD45 at activating and inhibitory human NK cell immune synapses. *J. Immunol.* 170:2862–2870.

44. Allenspach, E. J., P. Cullinan, J. Tong, Q. Tang, A. G. Tesciuba, J. L. Cannon, S. M. Takahashi, R. Morgan, J. K. Burkhardt, and A. I. Sperling. 2001. ERM-dependent movement of CD43 defines a novel protein complex distal to the immunological synapse. *Immunity.* 15:739–750.

45. Leupin, O., R. Zaru, T. Laroche, S. Müller, and S. Valitutti. 2000. Exclusion of CD45 from the T-cell receptor signaling area in antigen-stimulated T lymphocytes. *Curr. Biol.* 10:277–280.

46. Rees, D. A., C. W. Lloyd, and D. Thom. 1977. Control of grip and stick in cell adhesion through lateral relationships of membrane glycoproteins. *Nature.* 267:124–128.